Engineering with computers

Supplementary information

Toward engineering lattice structures with the Material Point Method (MPM)

Oliver Giraldo-Londoño[1], Rogelio A. Muñetón-López[1], Paul L. Barclay[2], Xiatian Zhuang[1], Duan Z. Zhang[2], Zhen Chen[1,3,✉]

[1] Department of Civil and Environmental Engineering, University of Missouri, Columbia, MO 65211, USA

[2] Theoretical Division, Fluid Dynamics and Solid Mechanics Group (T-3), Los Alamos National Laboratory, Los Alamos, NM 87545, USA

[3] Department of Mechanical and Aerospace Engineering, University of Missouri, Columbia, MO 65211, USA

Supplementary information

Toward engineering lattice structures with the Material Point Method (MPM)

Oliver Giraldo-Londoño[1], Rogelio A. Muñetón-López[1], Paul L. Barclay[2], Xiatian Zhuang[1], Duan Z. Zhang[2], Zhen Chen[1,3,✉]

S1. 3D model and 3D-printed lattice structure overview

Figure S1provides displays the 3D model used for the metamaterial prints, specifically showcasing a T2P30 lattice surrounded by support structures. The supports are designed to hold the lattice at a 30-degree angle during printing to minimize the impact of manufacturing imperfections. After the curing process, these supports are removed as part of the post-processing phase, and the lattices are then conditioned for further testing.

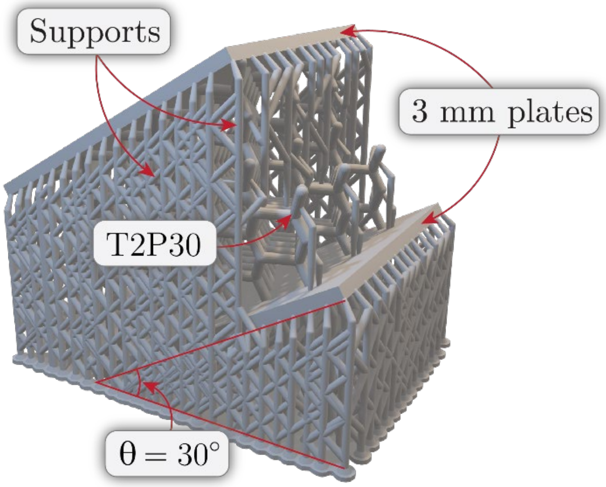

Figure S1. 3D model of the metamaterial lattice, showcasing a T2P30 lattice surrounded by support structures

Figure S2 shows an actual T2P30 3D-printed lattice structure at three different views. Each perspective provides a view of the complex geometric configuration of the lattices. Fig. S1 also provides a magnified view of one of the tetrahedral unit cells that conforms the lattice to show detailed measurements.

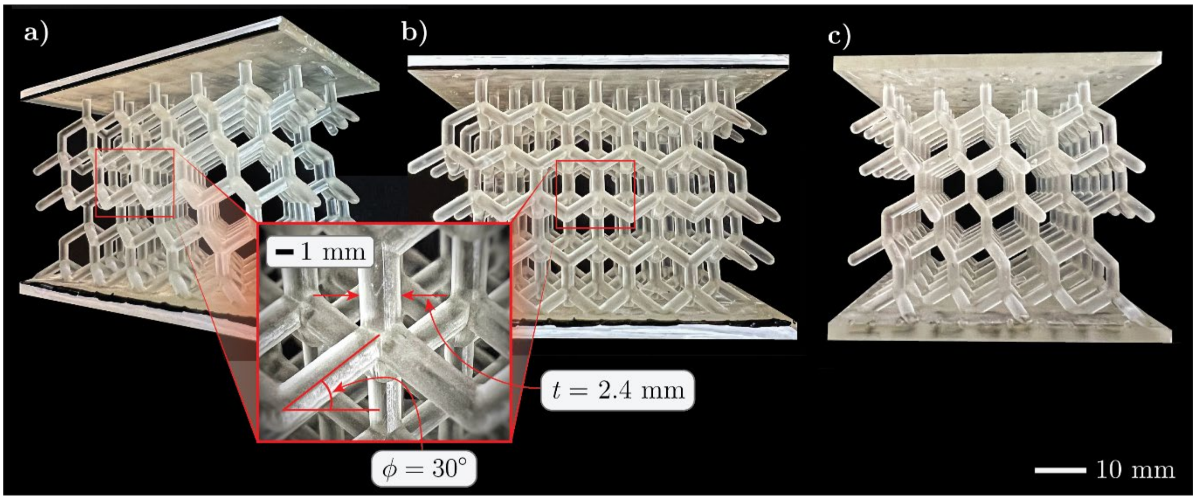

Figure S2. Different views of a 3D printed lattice T2P30. a) Isometric view, b) Front view, c) Lateral view

S2. Quasi-static compression testing on lattice structures

The quasi-static tests consisted of applying a controlled displacement with a constant rate of 0.05 mm/s on the top plate of the specimens until reaching a total deformation of 30 mm as shown in Figure S3. From these tests, we obtain compressive load–displacement curves which illustrate the response of the material under the applied load, which helped us gain insights into the mechanical behavior of these metamaterials. Furthermore, these tests helped identify the onset of buckling in some of the struts, localized material failure, and the point at which the structure densifies significantly, corresponding to the densification point.

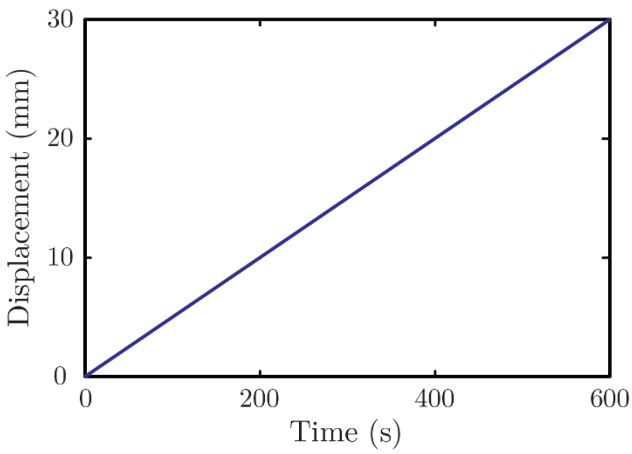

Figure S3. Displacement history applied in quasi-static tests

S3. Compression testing setup

The quasi-static compression tests were conducted using an ADMET universal testing machine. This machine is equipped with two flat plates that conform to the compression testing configuration, as depicted in Figure S4. This machine features a 2 kN capacity load cell to measures the reaction force at the top of the specimens and provides a controlled way to apply the displacement to the specimens. Additionally, the machine is equipped with a data acquisition (DAQ) which, throughout the duration of the tests, records real-time data including displacement, load, and time.

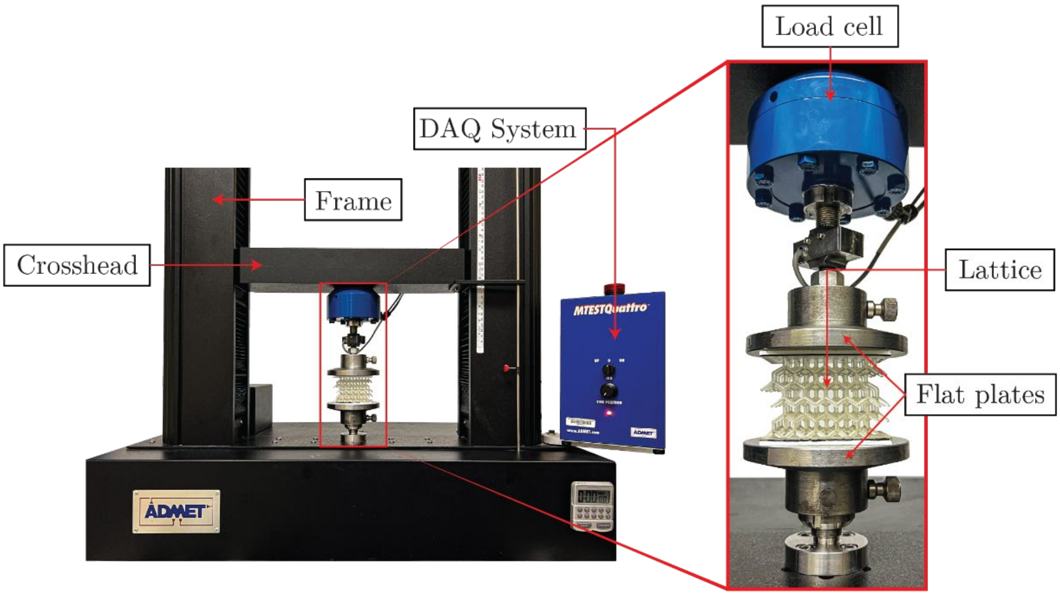

Figure S4. ADMET Universal testing machine used for quasi-static compression tests

S4. Characterization of base material

Figure S5 shows the cylindrical specimen used to characterize the base material in the same testing setup described above and the Stress vs. Strain curve obtained for a compression displacement of 0.003 mm/min.

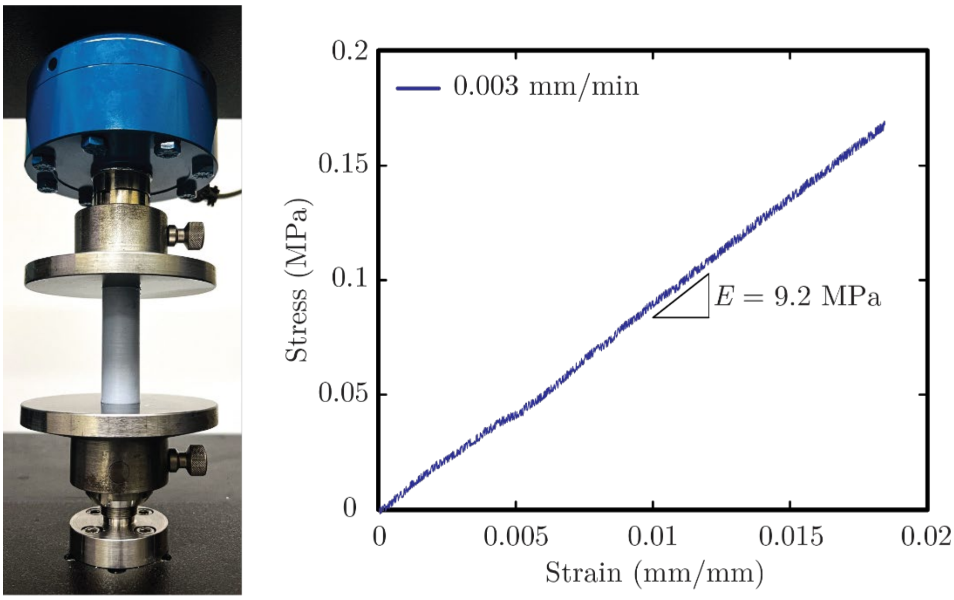

Figure S5. Characterization of base material. Testing setup (left), Stress vs. Strain response (right)

S5. Results of quasi-static testing of lattice structures

Figure S6 and Figure S7 show the quasi-static test at different times of the T1 and T2 lattices, respectively. As observed, by 120s, slight deformation is visible in all lattices, but it is more pronounced in the T1P20 lattice. By 300 s, buckling or initial buckling of several struts is evident in all the lattices. At 540 seconds, the P20 lattices exhibits nearly complete densification. This early densification can be attributed to the shallower angle, which under quasi-static loading offers less structural rigidity and allows a faster buckling of their elements. In contrast, the 30° and 40° lattices undergo a more gradual densification process under quasi-static loading.

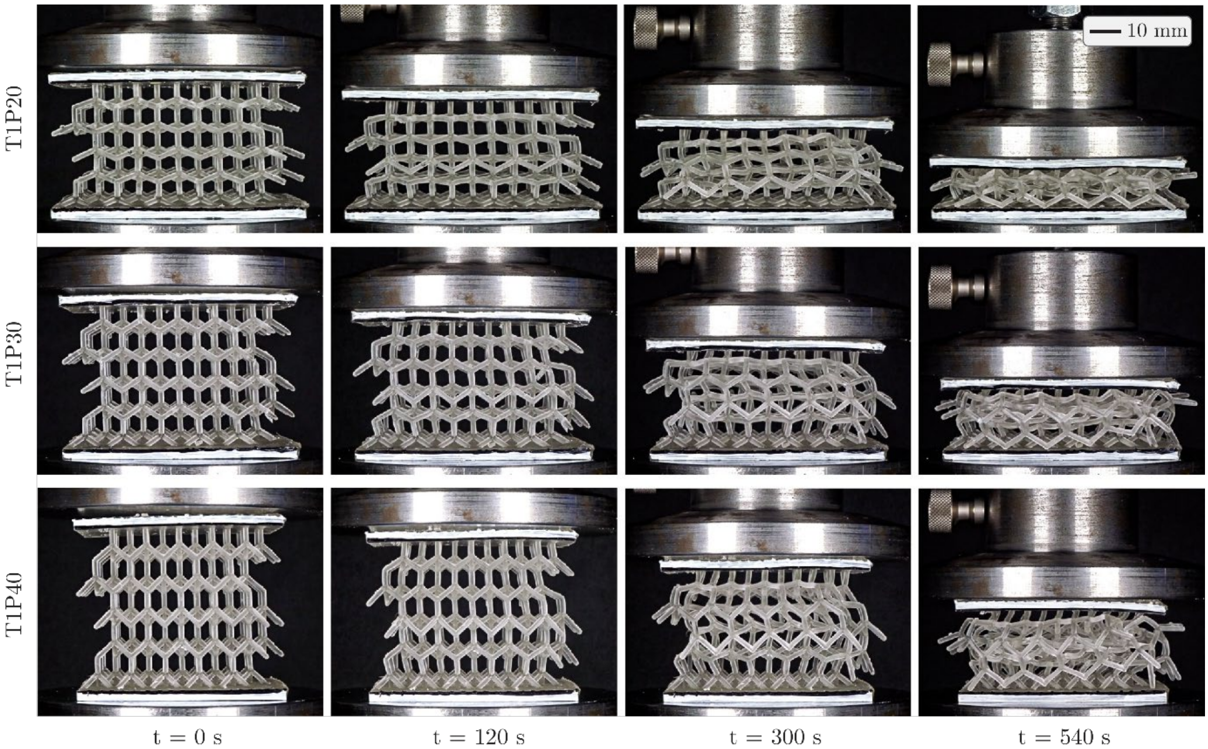

Figure S6. Quasi-static test of T1 lattices at different times

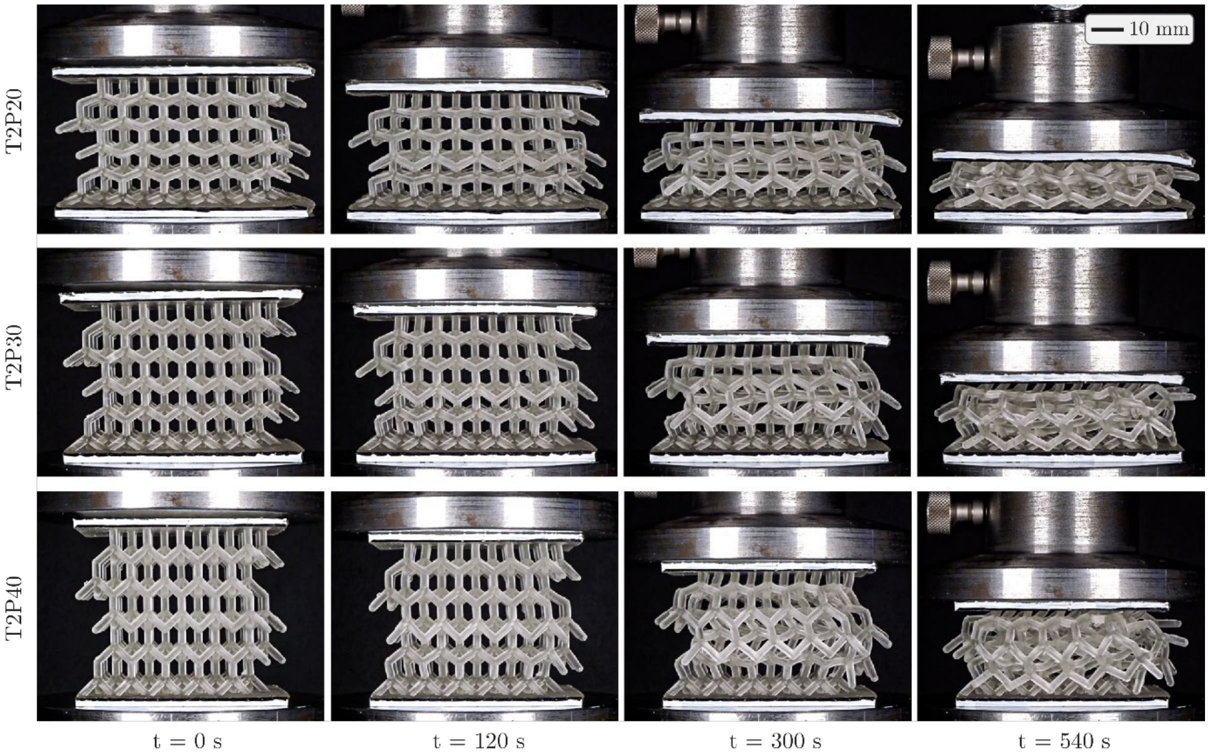

Figure S7. Quasi-static test of T2 lattices at different times

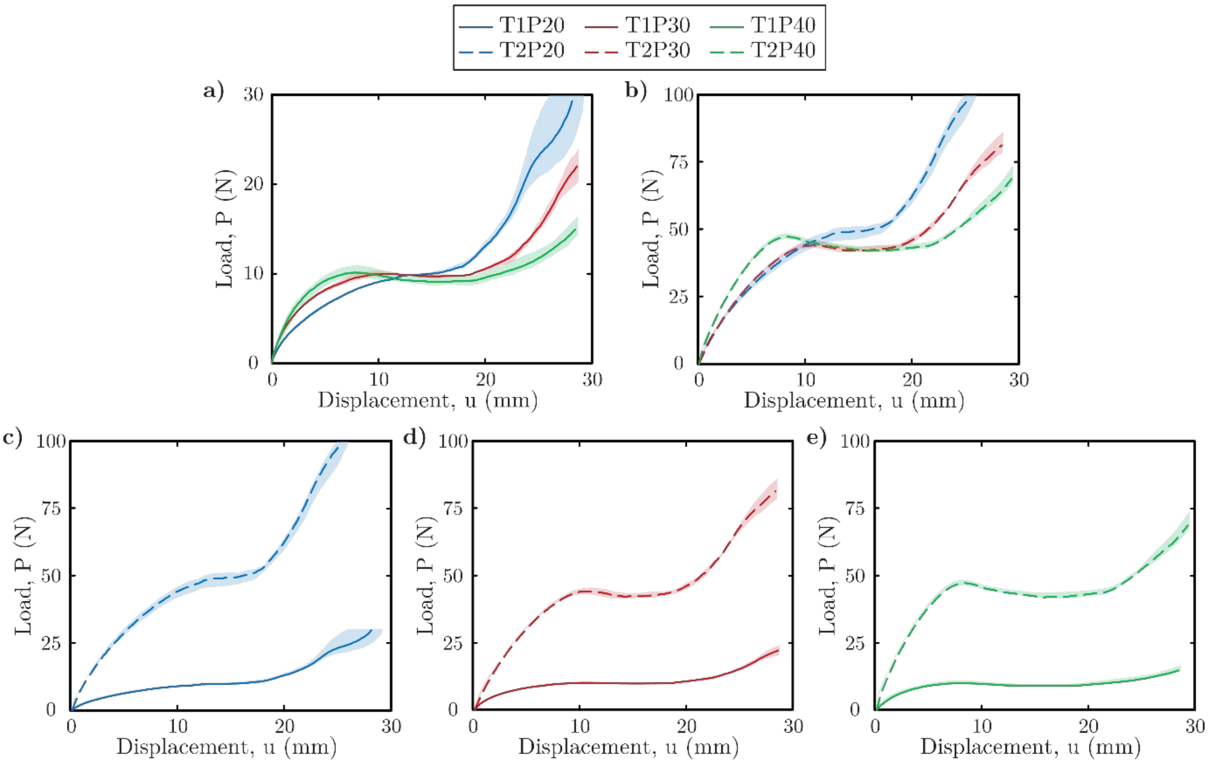

Figure S8. Load-displacement curves obtained from quasi-static tests. a) Summary of T1 lattices, b) summary of T2 lattices, c)-e) comparison of results for the different angles per type of lattice

Here we present the average post-processed data for each specimen type. Individual specimen results are omitted for brevity. Figure S8 summarize the results obtained for the various types of lattices under quasi-static loading. As observed from the plots, the general behavior of these lattices is characterized by a rapidly rapid increase in load until reaching the peak load (before softening), followed by a plateau region in which the lattices undergo significant deformation while the load presents small variations indicating a possible energy dissipation through controlled buckling of the struts. Beyond this point the load-displacement curves soften and then exhibits a steep upward trend as the structure densifies and transitions from a cellular to a more solid-like behavior.

S6. Verification of minimal plastic deformation in quasi-static compression tests

To address concerns regarding the assumption of purely elastic deformation in our simulations, we provide additional evidence through experimental data. Figure S9 presents sequential snapshots of the T1P30 lattice structure during the loading and unloading phases of a quasi-static compression test. The images demonstrate that the lattice structure returns to its original shape after the load is removed, indicating minimal plastic deformation. Correspondingly, Figure S10 shows the displacement-time response, where the displacement almost fully recovers after unloading, further supporting the negligible plasticity in the system under the quasi-static conditions evaluated in this study.

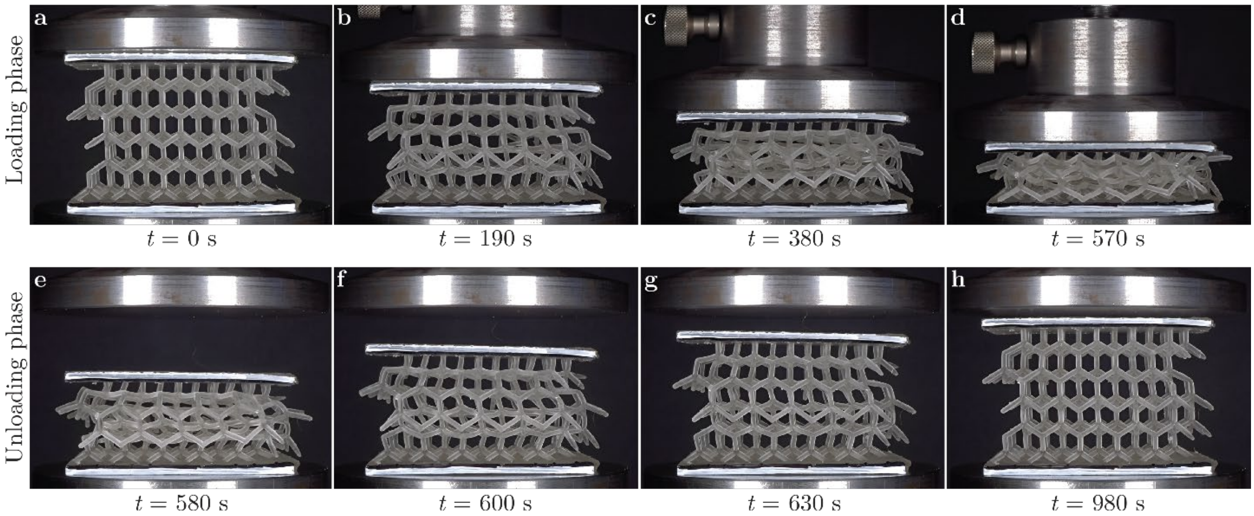

Figure S9. Sequential snapshots depicting the loading (a-d) and unloading (e-h) phases during a quasi-static compression test of the T1P30 lattice structure. The lattice undergoes progressive compression during the loading phase (a-d) and then gradually recovers its shape as the compressive force is released during the unloading phase (e-h).

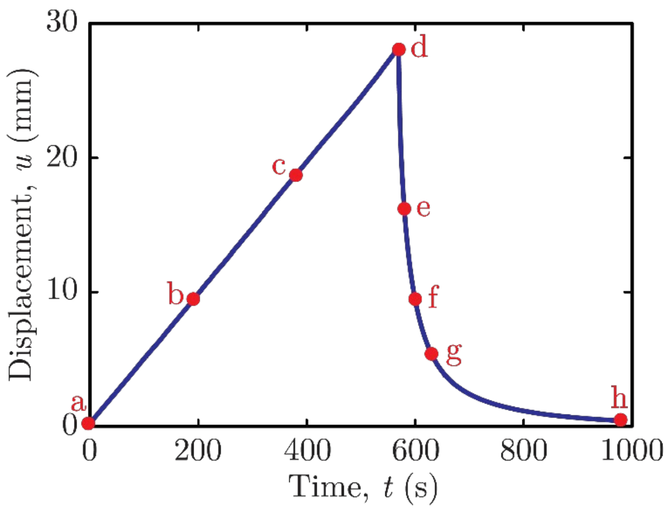

Figure S10. Displacement-time response corresponding to the loading (a-d) and unloading (e-h) phases of the T1P30 lattice structure during the quasi-static compression test. The plot illustrates the progressive increase in displacement during loading, followed by a decrease during unloading, with the displacement nearly returning to its initial value, indicating minimal permanent deformation.

S7. Comparison of deformation patterns, experimental vs. numerical results

Figure S11-16 compares the deformed shapes of each of the lattices at three deformation levels, u = 0, 10, and 20 mm, obtained experimentally (a) and with the DDMP (b) and GIMP (c) methods, respectively.

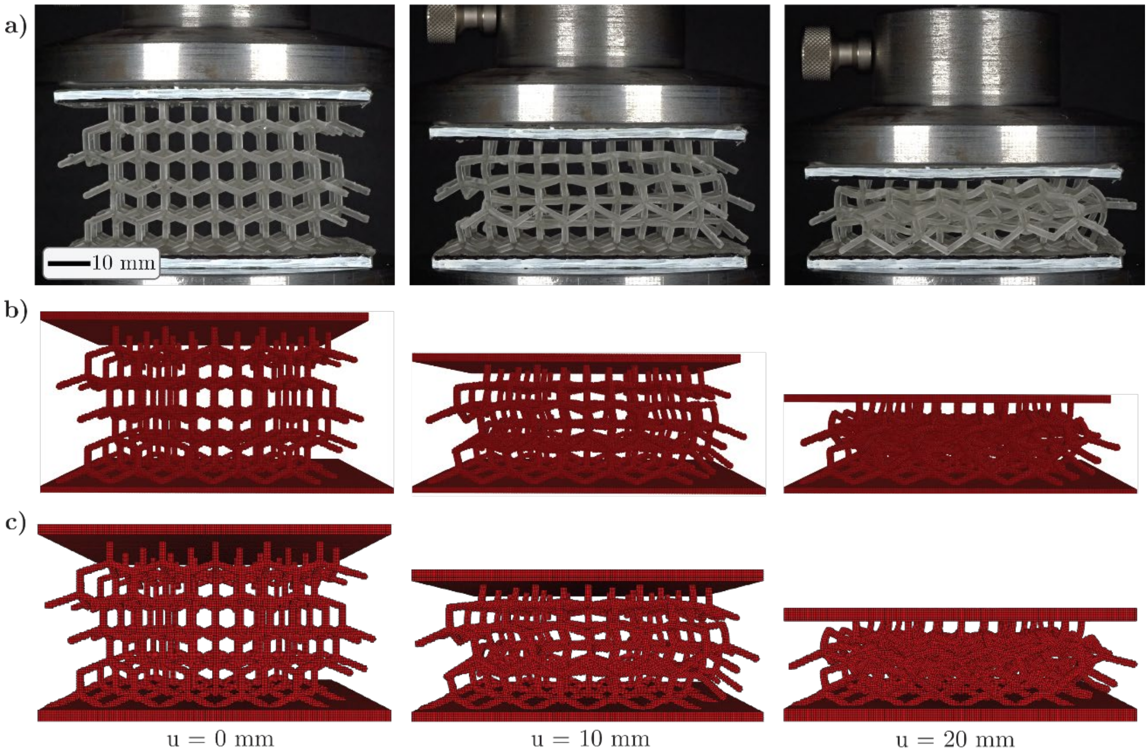

Figure S11. Progressive deformation of the T1P20 lattice structure at three different levels of deformation, u = 0, 10, and 20 mm. a) Experimental results, b) Results from the DDMP method, and c) Results from the GIMP method

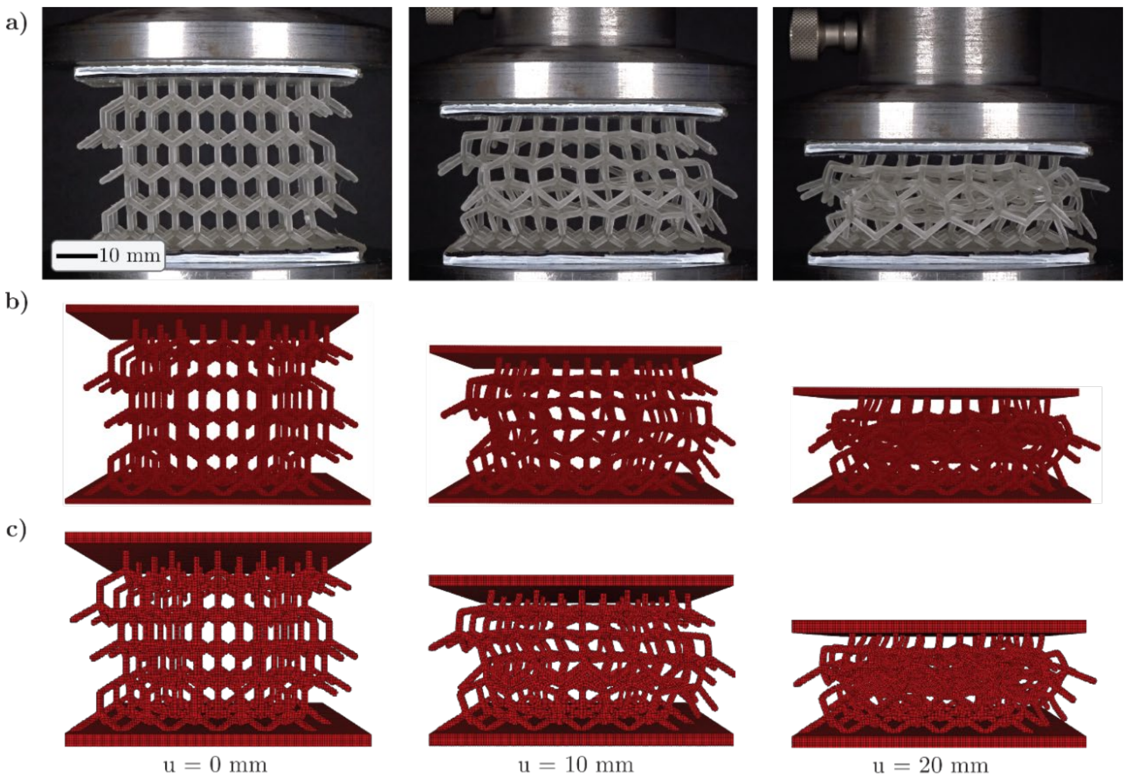

Figure S12. Progressive deformation of the T1P30 lattice structure at three different levels of deformation, u = 0, 10, and 20 mm. a) Experimental results, b) Results from the DDMP method, and c) Results from the GIMP method

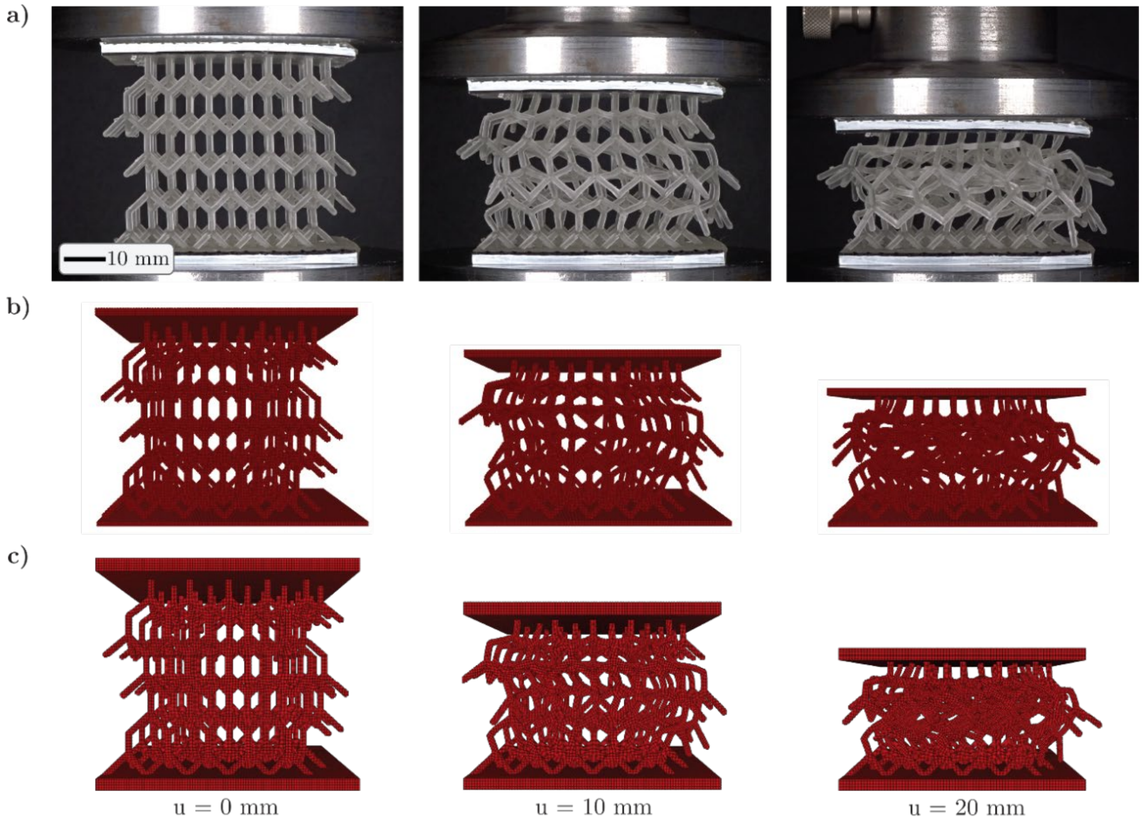

Figure S13. Progressive deformation of the T1P40 lattice structure at three different levels of deformation, u = 0, 10, and 20 mm. a) Experimental results, b) Results from the DDMP method, and c) Results from the GIMP method

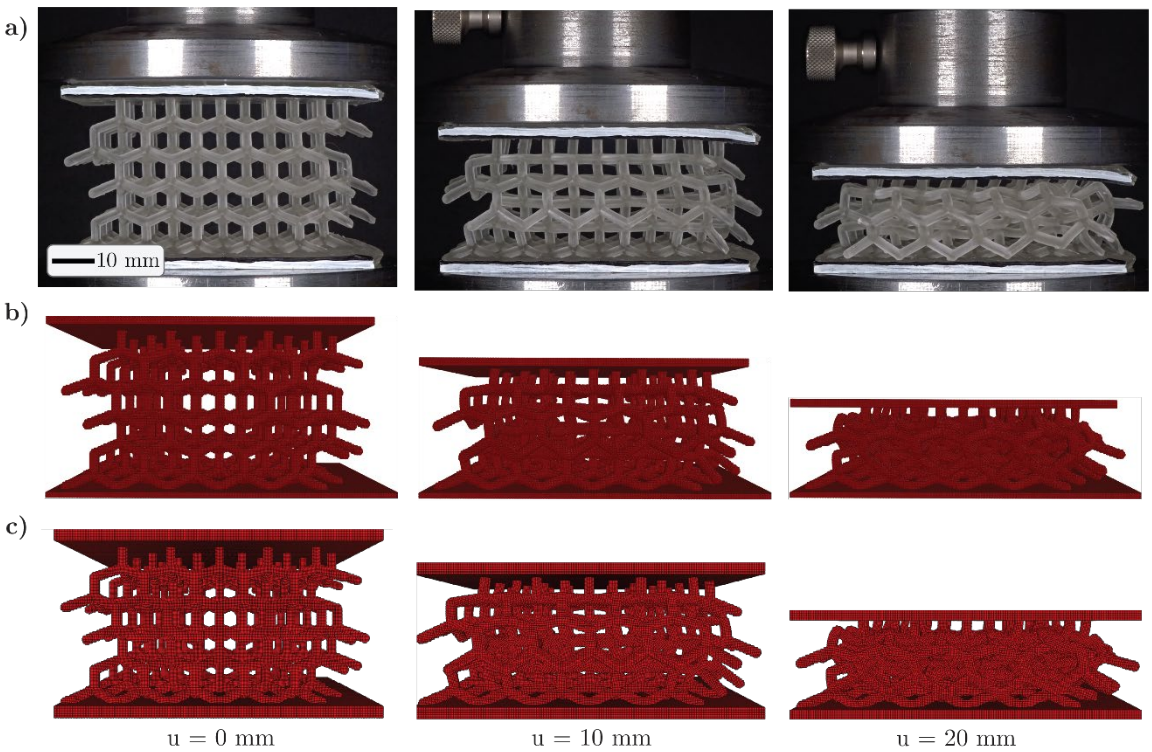

Figure S14. Progressive deformation of the T2P20 lattice structure at three different levels of deformation, u = 0, 10, and 20 mm. a) Experimental results, b) Results from the DDMP method, and c) Results from the GIMP method

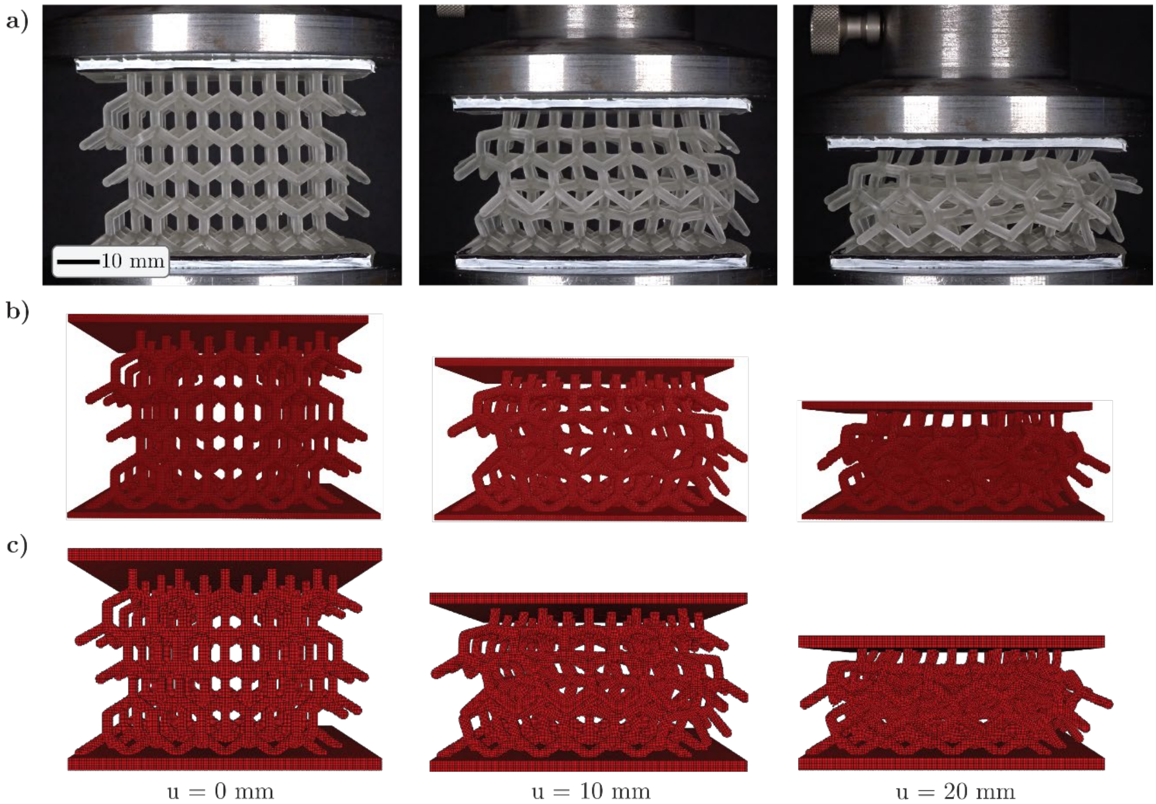

Figure S15. Progressive deformation of the T2P30 lattice structure at three different levels of deformation, u = 0, 10, and 20 mm. a) Experimental results, b) Results from the DDMP method, and c) Results from the GIMP method

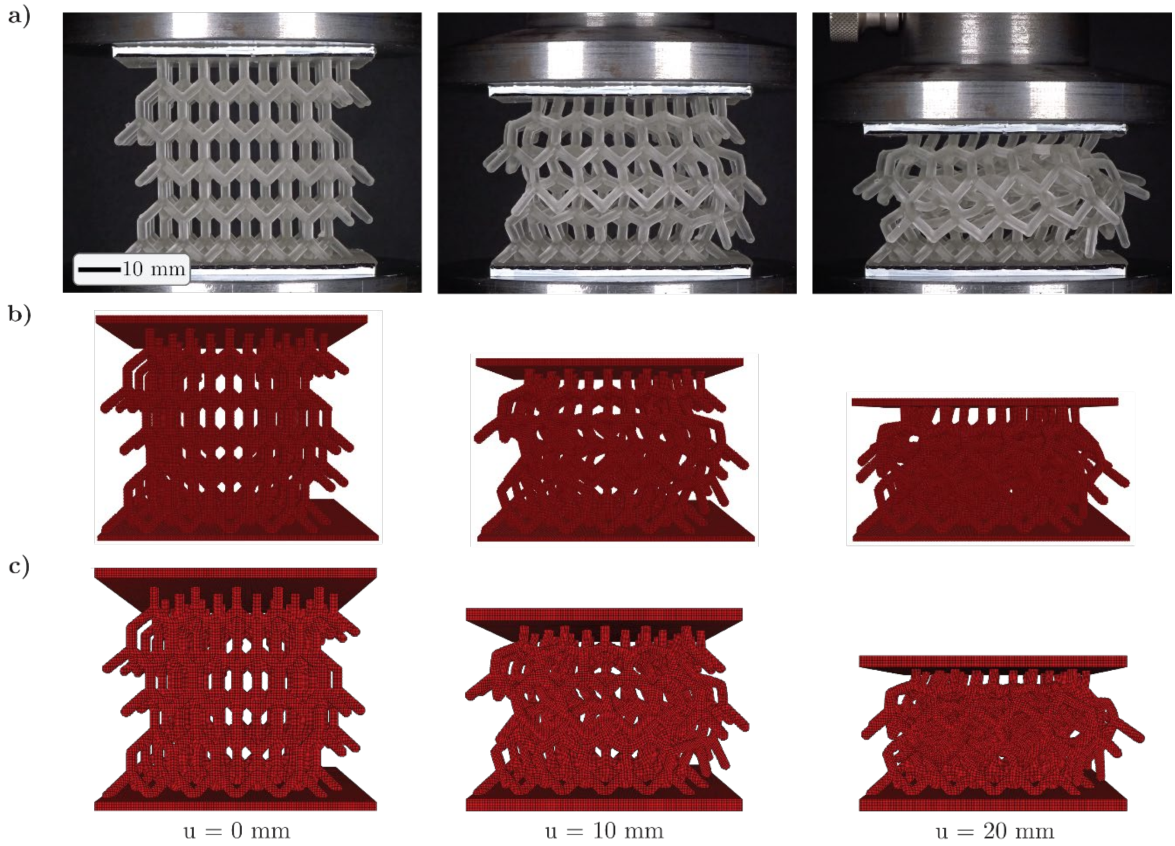

Figure S16. Progressive deformation of the T2P40 lattice structure at three different levels of deformation, u = 0, 10, and 20 mm. a) Experimental results, b) Results from the DDMP method, and c) Results from the GIMP method

S8. Numerical results for lattices with initial geometric imperfections - Additional Pertrubations

In addition to the four perturbations shown in the main paper, three additional perturbations were considered, which are as follows:

Perturbation E – Thinner plate region: This perturbation thinned the base layers, which reduces the number of material points and accelerates computational time, making simulations more efficient.

Perturbation F – Random material point deletion: This perturbation involved randomly removing material points from the main lattice structure and the base regions, simulating microscale voids that may arise during the manufacturing process. Simulations were done with a 2% deletion probability to account for these potential defects.

Perturbation G – Random distortion of material point positions: This perturbation involved distorting the initial material point positions of the lattice. This was done to better mirror the experimental setup as there may be slight imperfections in the manufacturing process causing the vertical members to not be perfectly aligned as in the original base configuration. Specifically, the initial positions of the material points were shifted in the x-, y-, and z-directions by amounts δ, where δ is a random number chosen from a Gaussian distribution with a width of 0.032 mm, which correspond to a width of 10% of the particle spacing.

Each of these perturbations had negligible impact in the complete load-displacement response, suggesting accurate modeling of the compression plate and minimal effect from small defects or voids in individual unit cells. Thus, the motivation for not including perturbations E-G in the main work.

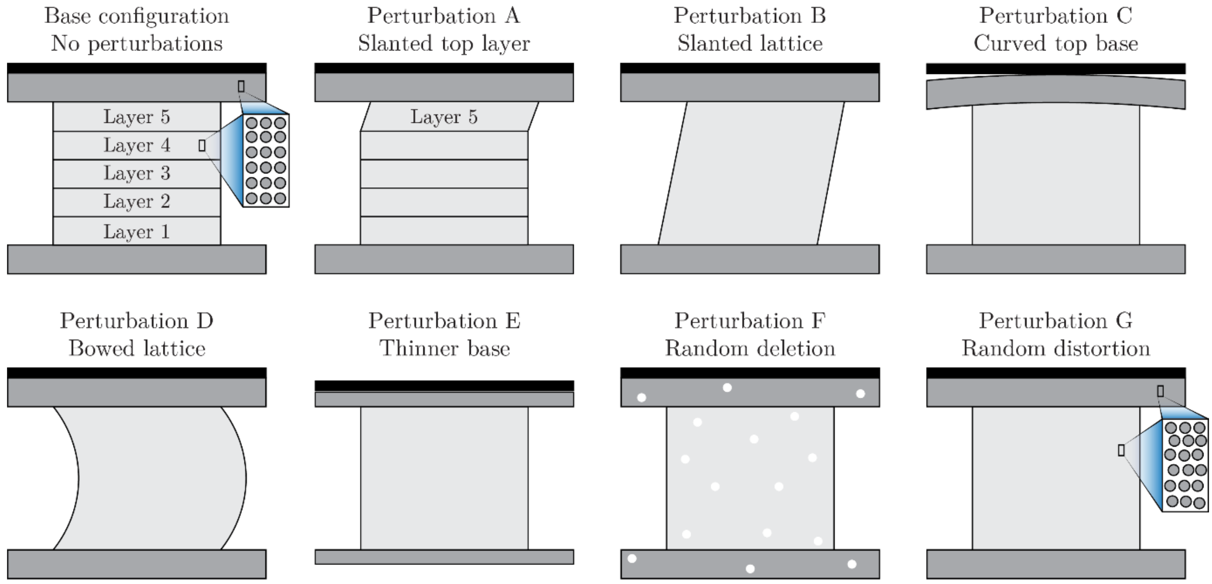

Figure S17. Base lattice configuration along with the seven different types of perturbations (A-G) studied in the geometric imperfections analysis of lattices

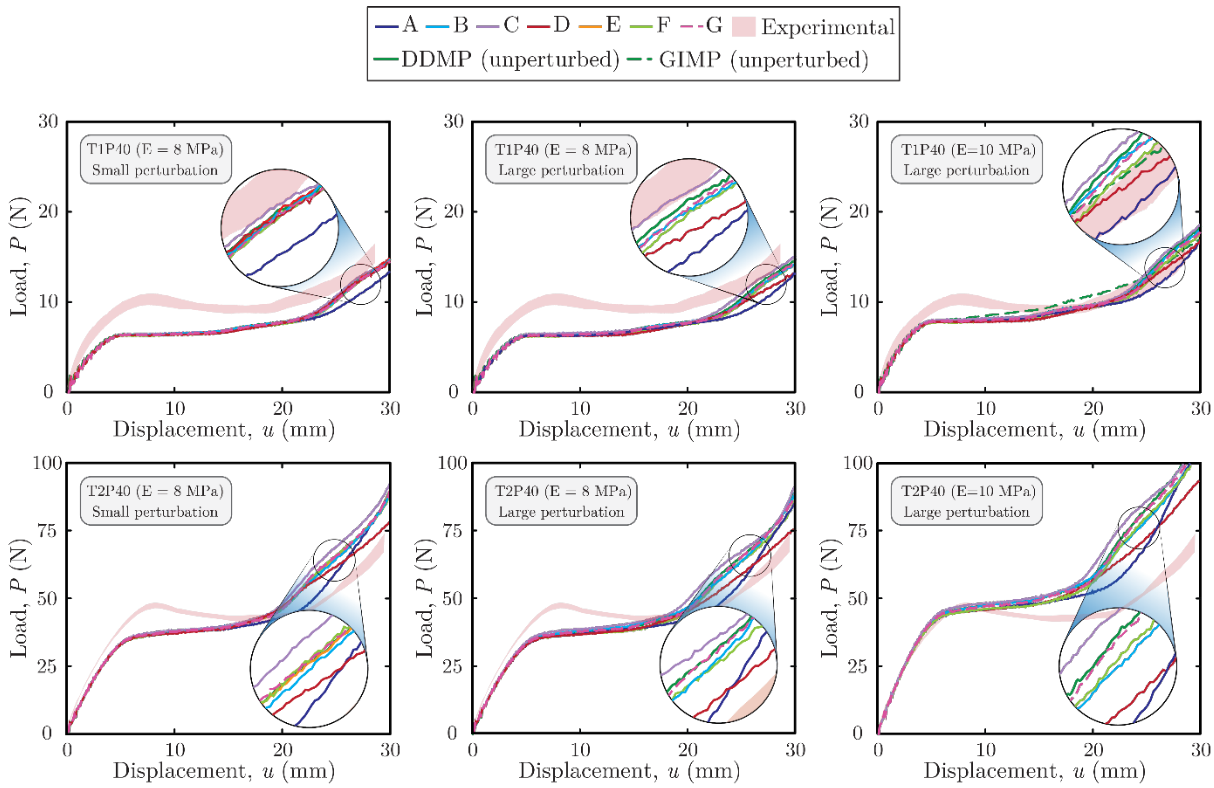

Figure S18. Load-displacement curves obtained from the geometric imperfection analysis of the T1P40 and T2P40 lattices considering all cases